7. Finite Difference Method (FDM)

7.1. Introduction

In the preceding review of electromagnetic theory the basic partial differential equations mathematically describing the phenomena of electromagnetic fields were shown. Along with those equations various different boundary conditions were introduced and associated to them forming so called boundary value problems (BVPs). An analytical way of solving such BVPs has also been shown. It was obvious that this method is unfortunately restricted to the narrow set of problems with a high level of geometrical symmetry, usually homogenous materials and very simple boundary conditions. Hence, it is clear that for real-life problems with complex geometries, nonlinear/inhomogeneous materials and arbitrary boundary conditions one has to use something more powerful than analytical methods to solve BVP. Due to their flexibility, adaptivity and generality, numerical methods for solution of the partial differential equations (PDFs) of electromagnetic field theory are powerful enough to solve practical problems involving all the mentioned difficulties. Along with modern powerful PC architectures and well educated experts, numerical methods offer practically unlimited capabilities in producing cheap and accurate digital prototypes of devices based on modern technology (lasers, satellite equipment, nano-electronics etc.).
The Finite Difference Method (FDM) in its primitive form was developed in the 1920s [1]. At that time it was called "the method of squares" and was used for solving nonlinear hydrodynamic equations. FDM is based on the approximation of partial derivatives by using finite differences. In this way, partial differential equations are replaced by finite difference equations that are of algebraic form. This chapter is organized as a review of FDM applications on various types of PDEs and with a particular stress on electrodynamics.

7.2. Finite Difference Schemes

As was already mentioned, the finite difference algorithm is based on the approximation of partial derivatives by finite differences. In order to illustrate this concept we will analyze a scalar function of 3 spatial variables:

$$\Phi(\vec{r}) = \Phi(x, y, z) \tag{7.1}$$

The partial derivative of function $\Phi(x, y, z)$ with respect to variable x, for example can be approximated using the so-called *forward-difference formula* at the point x_0 as follows [2, 4]:

$$\frac{\partial \Phi}{\partial x}(x_0, y_0, z_0) \approx \frac{\Phi(x_0 + h_x, y_0, z_0) - \Phi(x_0, y_0, z_0)}{h_x} \tag{7.2}$$

or *the backward-difference formula* [2, 4]:

$$\frac{\partial \Phi}{\partial x}(x_0, y_0, z_0) \approx \frac{\Phi(x_0, y_0, z_0) - \Phi(x_0 - h_x, y_0, z_0)}{h_x} \tag{7.3}$$

or *the central-difference formula* [2, 4]:

$$\frac{\partial \Phi}{\partial x}(x_0, y_0, z_0) \approx \frac{\Phi(x_0 + h_x, y_0, z_0) - \Phi(x_0 - h_x, y_0, z_0)}{2h_x} \tag{7.4}$$

where h_x represents the difference of variable x, i.e. $h_x = \Delta x$.
The second partial derivative of our scalar function with respect to variable x can be approximated in a similar way:

$$\frac{\partial^2 \Phi}{\partial x^2}(x_0, y_0, z_0) \overset{Backward}{\approx} \frac{\frac{\partial \Phi}{\partial x}(x_0, y_0, z_0) - \frac{\partial \Phi}{\partial x}(x_0 - h_x, y_0, z_0)}{h_x} \overset{Forward}{\approx}$$
$$\overset{Forward}{\approx} \frac{\frac{\Phi(x_0 + h_x, y_0, z_0) - \Phi(x_0, y_0, z_0)}{h_x} - \frac{\Phi(x_0, y_0, z_0) - \Phi(x_0 - h_x, y_0, z_0)}{h_x}}{h_x} \tag{7.4}$$

After some basic mathematical manipulation the second partial derivative can be written:

$$\frac{\partial^2 \Phi}{\partial x^2}(x_0, y_0, z_0) \approx \frac{\Phi(x_0 + h_x, y_0, z_0) - 2 \cdot \Phi(x_0, y_0, z_0) + \Phi(x_0 - h_x, y_0, z_0)}{h_x^2} \tag{7.5}$$

The presented method of partial derivative approximation is rather intuitive but has unknown accuracy. A more appropriate analysis that can lead to these formulas as well as their accuracies can be performed using the theory of Taylor's expansion. Namely, according to Taylor's theory the following can be written:

$$\Phi(x_0 + h_x, y_0, z_0) = \Phi(x_0, y_0, z_0) + \frac{h_x}{1!}\frac{\partial \Phi}{\partial x}(x_0, y_0, z_0) + \frac{h_x^2}{2!}\frac{\partial^2 \Phi}{\partial x^2}(x_0, y_0, z_0) +$$
$$+ \frac{h_x^3}{3!}\frac{\partial^3 \Phi}{\partial x^3}(x_0, y_0, z_0) + O_1(h_x^4) \tag{7.5.1}$$

$$\Phi(x_0 - h_x, y_0, z_0) = \Phi(x_0, y_0, z_0) - \frac{h_x}{1!}\frac{\partial \Phi}{\partial x}(x_0, y_0, z_0) + \frac{h_x^2}{2!}\frac{\partial^2 \Phi}{\partial x^2}(x_0, y_0, z_0) -$$
$$- \frac{h_x^3}{3!}\frac{\partial^3 \Phi}{\partial x^3}(x_0, y_0, z_0) + O_2(h_x^4) \tag{7.5.2}$$

If we add equations (7.5.1) and (7.5.2) we obtain:

$$\Phi(x_0 + h_x, y_0, z_0) + \Phi(x_0 - h_x, y_0, z_0) = 2 \cdot \Phi(x_0, y_0, z_0) + h_x^2 \frac{\partial^2 \Phi}{\partial x^2}(x_0, y_0, z_0) + O(h_x^4) \tag{7.5.3}$$

$$\frac{\partial^2 \Phi}{\partial x^2}(x_0, y_0, z_0) = \frac{\Phi(x_0 + h_x, y_0, z_0) - 2 \cdot \Phi(x_0, y_0, z_0) + \Phi(x_0 - h_x, y_0, z_0)}{h_x^2} + O(h_x^2) \tag{7.5.4}$$

Equation (7.5.4) confirms equation (7.5) and shows that the accuracy of that approximation is $O(h_x^2)$. If we subtract equations (7.5.1) and (7.5.2) we obtain:

$$\Phi(x_0 + h_x, y_0, z_0) - \Phi(x_0 - h_x, y_0, z_0) = 2 \cdot \frac{h_x}{1!}\frac{\partial \Phi}{\partial x}(x_0, y_0, z_0) + O(h_x^3) \tag{7.5.5}$$

$$\frac{\partial \Phi}{\partial x}(x_0, y_0, z_0) = \frac{\Phi(x_0 + h_x, y_0, z_0) - \Phi(x_0 - h_x, y_0, z_0)}{2 \cdot h_x} + O(h_x^2) \tag{7.5.6}$$

Equation (7.5.6) proves the central-difference formula (7.4) and shows that it has an accuracy of the order of $O(h_x^2)$. As opposed to the central-difference formula (7.4), by performing a similar analysis to (7.1-5.6), it is possible to show that the forward- and backward-difference formulas (7.2, 7.3) have an accuracy of $O(h_x)$. Information on the accuracy of a certain approximation will be very important in the analysis later on.
In a similar manner one can approximate the partial derivatives with respect to variables *y* and *z*. Having equations (7.2, 7.3, 7.5), we can also approximate the partial differential equations that describe a certain physical process such as the temperature distribution, electrostatic field or electromagnetic wave propagation. This procedure is called the discretization of PDEs using the FD algorithm. In the remaining sections we will use this algorithm to solve elliptic, parabolic and hyperbolic PDEs.

7.3. Parabolic PDEs and FDM (2D Transient Thermal Analysis)

Let us consider a 2d example of the transient thermal analysis depicted in the Figure 7.1. Namely, we will analyze the problem of temperature distribution in an iron body with an initial temperature of 0˚C (an initial condition at $t = 0s$). From the beginning of our observation the left-hand side of the body is exposed to boiling water (100 ˚C) while the right-hand side is in contact with a block of ice (0 ˚C). The lateral surfaces of the iron body are perfectly insulated in a thermal sense from outer space (no flow of thermal energy is possible). Such a transient heat conduction problem can be mathematically formulated as follows [3]:

$$\frac{\partial}{\partial x}\left(\lambda_x \frac{\partial T}{\partial x}\right)+\frac{\partial}{\partial y}\left(\lambda_y \frac{\partial T}{\partial y}\right)=\rho \cdot c_p \cdot \frac{\partial T}{\partial t} \text{ in } \Omega \subseteq R^2 \tag{7.6}$$

$$T = T_D, \text{ over } \partial_D\Omega \tag{7.7}$$

$$\frac{\partial T}{\partial n} = 0, \text{ over } \partial_N\Omega \tag{7.8}$$

$$T = 0, \text{ everywhere at } t = 0 \tag{7.9}$$

Equation (7.6) is a PDE describing the transient heat conduction in a solid body[1]. The Dirichlet boundary conditions (prescribed temperature) are given over the Dirichlet boundary as in (7.7) and the Neumann boundary conditions (prescribed heat flux) are defined over the Neumann part of the boundary as in (7.8). The coefficients appearing in (7.6-7.9) are as follows:

λ_x, λ_y	- thermal conductivities (W/mK) in the *x* and *y* directions respectively
ρ	- density (kg/m^3)
c_p	- specific heat capacity (J/kgK)
$T = T(x, y, t)$	- temperature as a function of position and time
T_D	- fixed value of temperature over the Dirichlet part of the boundary

[1] It is called a parabolic PDE

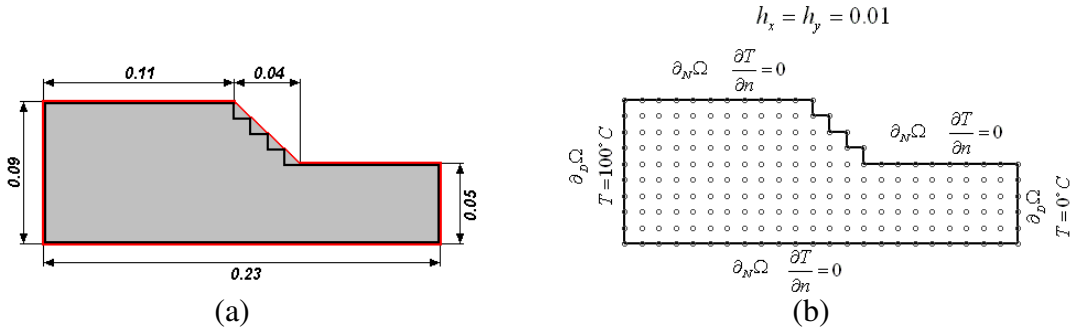

Figure 7.1. 2D heat conduction problem geometry, grid and BC definition;
(a) geometrical definition of the computational domain (all dimensions are given in meters)
(b) BC and FD grid definition (grid is equidistant in *x* and *y* direction, $h_x = h_y$)

The first step in the application of FDM to the transient heat conduction problem described by (7.6-7.9) is to define a regular grid over the computational domain. As one can see in Figure 7.1a the geometry of our heat conduction problem (red solid line) is very simple. The regular grid that is needed for FDM obviously can not accurately describe the parts of domain containing slopes. The FDM grid approximates those parts by stair-like subdomains as can be seen in Figure 7.1a (black solid line). This is the basic drawback of FDM and of other methods that use a regular grid. However, if the grid is more dense the approximation of slopes is better. The second step is to choose a kind of representation for the differential operators by their finite difference approximations. In order to have a clear and simple notation it is very useful to introduce a FD notation convention that operates only with integer indexes representing points in the grid (both in space and in time). Namely, if our grid is equidistant (constant step) the position of a node in the space-time grid is determined by 3 integer numbers:

$$(x_i, y_j, t_k) = (x_0 + i \cdot \Delta x, y_0 + j \cdot \Delta y, t_0 + k \cdot \Delta t) \overset{(FD\ notation)}{\sim} (i, j, k) \tag{7.10}$$

where $i = 0,1,2,\ldots$, $j = 0,1,2,\ldots$, and $k = 0,1,2,\ldots$ The space-time grid is defined by its steps Δx, Δy, Δt on the *x*, *y* and *t* axes respectively.

Let us now write the approximation of the differential operators of equation (7.6) by means of notation (7.10) and formulas (7.2) and (7.5). This goes as follows:

$$\frac{\partial T}{\partial t}(x, y, t) \overset{(2),(10)}{\approx} \frac{T(i, j, k+1) - T(i, j, k)}{\Delta t} \tag{7.11}$$

$$\frac{\partial^2 T}{\partial x^2}(x, y, t) \overset{(5),(10)}{\approx} \frac{T(i+1, j, k) - 2 \cdot T(i, j, k) + T(i-1, j, k)}{(\Delta x)^2} \tag{7.12}$$

$$\frac{\partial^2 T}{\partial y^2}(x, y, t) \overset{(5),(10)}{\approx} \frac{T(i, j+1, k) - 2 \cdot T(i, j, k) + T(i, j-1, k)}{(\Delta y)^2} \tag{7.13}$$

With the help of (7.12) and (7.13), the second partial derivatives of the temperature with respect to *x* and *y* are approximated. If we have a look at equation (7.6), its left-hand side can

be obtained in simple form only if the material is homogenous[2] and isotropic[3]. Having approximation (7.11-7.13), equation (7.6) can be approximated by the following finite difference scheme:

$$\lambda\frac{T(i+1,j,k)-2\cdot T(i,j,k)+T(i-1,j,k)}{(\Delta x)^2}+\lambda\frac{T(i,j+1,k)-2\cdot T(i,j,k)+T(i,j-1,k)}{(\Delta y)^2}= \\ =\rho\cdot c_p\cdot\frac{T(i,j,k+1)-T(i,j,k)}{\Delta t} \tag{7.14}$$

where k is $\lambda=\lambda_x=\lambda_y$. If the grid is equidistant in terms of x and y variables, i.e. if $\Delta x=\Delta y$ it is useful to define:

$$r=\frac{\Delta t\cdot\lambda}{\rho\cdot c_p\cdot\Delta x^2} \tag{7.15}$$

Equation (7.14) can be simplified using (7.15) and transformed into a more appropriate form by keeping only the term $T(i,j,k+1)$ on the left-hand side. This is a logical progression because the solution of the proceeding step should be obtained using the solution of the previous step (explicit approach). The solution of the first step is obtained in terms of boundary and initial conditions. Hence the **explicit formula** has the following form:

$$T(i,j,k+1)=(1-4r)T(i,j,k)+r\left[T(i+1,j,k)+T(i-1,j,k)+T(i,j+1,k)+T(i,j-1,k)\right] \tag{7.16}$$

Up to now it is clear that having the grid and formula (7.16) one can iteratively compute the unknown scalar field (temperature) for a sequence of instants in time obtaining a sequence of solutions in space. At this point it is important to say something about the boundary conditions and their influence on our explicit formula. As one can see from (7.16), in order to compute the new field at a certain point in the spatial grid it is necessary to know the old field in all 4 surrounding points[4]. The question is: what to do at points on the boundary where, depending on the situation, only 3 or even 2 neighbours exist? For Dirichlet's type of BC (7.7) the situation is clear: the field has a fixed value for all time steps. For Neumann's type of BC the situation is a bit more complicated. In this case the following has to be performed:

$$\frac{\partial T}{\partial n}=\left(\frac{\partial T}{\partial x}\vec{e}_x+\frac{\partial T}{\partial y}\vec{e}_y\right)\cdot\vec{n}\overset{(8)}{=}0 \tag{7.17}$$

Depending on the situation, vector $\vec{n}$ can be parallel to the x or y axis. In addition to these 2 cases, there is also the possibility that $\vec{n}$ is perpendicular to the diagonal of the grid cell representing a single step of the slope. Using (7.2), (7.17) and the assumption of an equidistant grid in terms of x and y for all 3 cases it is possible to write:

$$T(i+1,j,k)=T(i,j,k),\ \text{for}\ \vec{n}=\vec{e}_x \tag{7.18}$$

$$T(i,j+1,k)=T(i,j,k),\ \text{for}\ \vec{n}=\vec{e}_y \tag{7.19}$$

---

[2] In homogenous material thermal conductivities do not depend on position, i.e. $k_x\neq k_x(x,y)$, $k_y\neq k_y(x,y)$

[3] In isotropic material thermal conductivities do not depend on direction, i.e. $k_x=k_y$

[4] "New" and "old" are understood here in the sense of time steps

$$T(i+1,j,k)+T(i,j+1,k)=2\cdot T(i,j,k)\text{ , for }\vec{n}=\frac{\sqrt{2}}{2}\left(\vec{e}_x+\vec{e}_y\right) \tag{7.20}$$

Depending on the situation, one can use (7.18), (7.19) or (7.20) to replace the missing terms in the explicit formula (7.14) for the case of nodes with Neumann BC.
Up to now the FD scheme was clarified and aspects of implementation of various BC have been discussed. Only the details of grid generation remain to be explained. The grid density in terms of space is determined by the required accuracy. Namely, if our geometry is a very detailed one, a more detailed (higher resolution) grid is required, i.e. more points are required. Having a defined spatial grid, one also has to choose the time step for the explicit formula. This part requires more experience because of **stability problems**. At first sight it looks like the time step is determined only by our requirement for the time resolution of the obtained data, i.e. by our need to have results at certain moments in time. This is not so in reality. Namely, long ago, at the very beginning of the application of this method (FDM), it was observed that if the time step is not small enough the behaviour of the explicit equation (7.14) becomes unpredictable and the resulting solution unbounded. This is called instability. What causes instability? The answer is not simple. If one defines the grid and applies an explicit formula to it, an achieved solution after a certain number of steps has a certain accuracy. The accuracy is usually quantified by the relative error (norm of disagreement between numerical solution and exact solution divided by the norm of exact solution). If one wants to increase the accuracy it is usually necessary to refine the grid and consequently the **truncation error** as well. This can not be done indefinitely because a grid with higher resolution requires more mathematical operations to be done at each time step, which consequently increases the **round-off error**. These two opposite tendencies allow us to achieve the accuracy of a solution only up to a certain level (minimum of their superposition) and more than that can not be achieved. The truncation error and the round-off error together determine the stability of the explicit scheme (7.14). Namely, it is useful to define the following [4]:

$$\varepsilon^{n+1}=g\cdot\varepsilon^{n} \tag{7.21}$$

where ε^{n+1} is the error of the solution at time step $(n+1)$, ε^{n} is the error of the solution at time step (n) and g is an amplification factor.
For stability of scheme (7.14) it is necessary that the following condition holds:

$$\left|\varepsilon^{n+1}\right|\le\left|\varepsilon^{n}\right|\ \Rightarrow\ |g|\le 1 \tag{7.22}$$

In the case of explicit scheme (7.14), one can perform the Fourier analysis of it in order to find an amplification factor. In this way, according to source [4], it can be shown that the stability condition for scheme (7.14) is as follows:

$$0<r\le\frac{1}{4} \tag{7.23}$$

In order to have stability for the explicit algorithm, one has to initially define a spatial grid resolution with respect to the model geometry and desired accuracy (truncation error) and then calculate the maximum possible value of time step using (7.23).
After this review of theory, let us now go back to our example of heat transfer depicted in Figure 7.1. The material of the solid body is, for example, pure iron. This material, according to reference [5], has the following properties:

$$c_p = 444\,\frac{J}{kg\cdot K},\ \rho = 7870\,\frac{kg}{m^3},\ k = 80.2\,\frac{W}{m\cdot K} \tag{7.24}$$

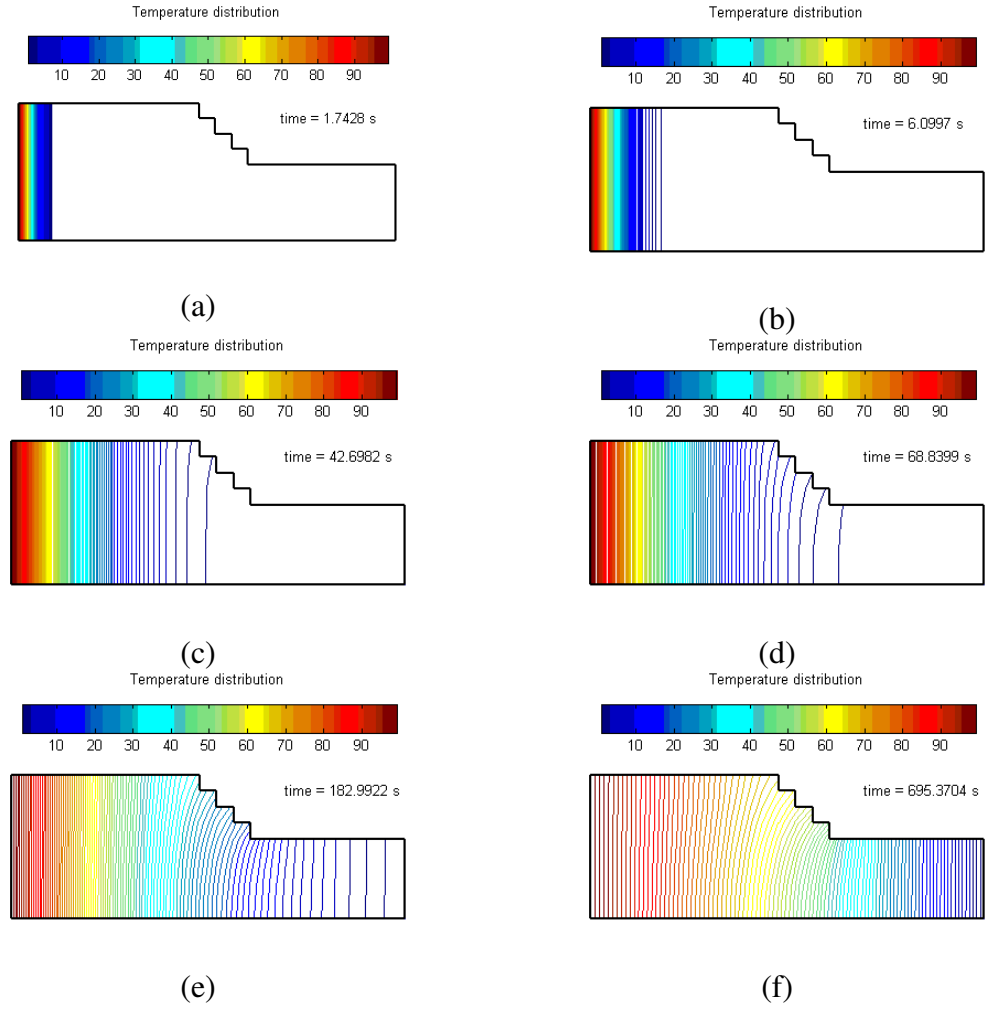

Figure 7.2. Solution of transient 2D heat conduction problem for various different instants of time is presented; At the very beginning the temperature rise is located in the narrow area around the hot boundary (a); As time goes by the temperature rise affects a larger area (b-e); After more than 10 minutes a stationary situation was established (f).

For the spatial grid the grid constant was chosen to be $\Delta x = \Delta y = 0.01\ m$. A graphical representation of this grid is given in Figure 7.1b. Having the definition of the spatial grid and the properties of the material (7.24), it is possible to compute a critical or maximal time step regarding stability:

$$r_{\max} \overset{(23)}{=} 0.25 \overset{(15)}{\Rightarrow} \quad \frac{\Delta t_{\max}\cdot k}{\rho\cdot c_p\cdot \Delta x^2} = 0.25 \Rightarrow\ \Delta t_{\max} = 0.25\cdot\frac{\rho\cdot c_p\cdot \Delta x^2}{k} = 1.0892\ s \tag{7.25}$$

For an initial calculation it is reasonable to ensure stability by imposing a “security” factor:

$$\Delta t = 0.8\cdot\Delta t_{\max} = 0.8714\ s \tag{7.26}$$

The first calculation is performed with the time step (7.26) and the results are given in Figure 7.2 for various instants in time.
Let us see now what happens when the stability condition is not fulfilled. Namely instead of a security factor of 0.8 in (7.26), one can simply use a factor of 1.2 and be in the range of instability:

$$\Delta t = 1.2 \cdot \Delta t_{\max} = 1.30704\ s \tag{7.27}$$

Using the same code, that produced the nice results depicted in Figure 7.2 with time step (7.26), one can not produce any reasonable result with time step (7.27). This is shown in Figure 7.3. Although everything looks normal at the beginning (a-c), after a sufficient number of iterations, the field becomes disturbed (d) and later even obviously wrong (e, f). This shows that the stability of the explicit FD method for parabolic PDEs plays an important role and requires a calculation of critical time step (stability condition) for each particular case of application.

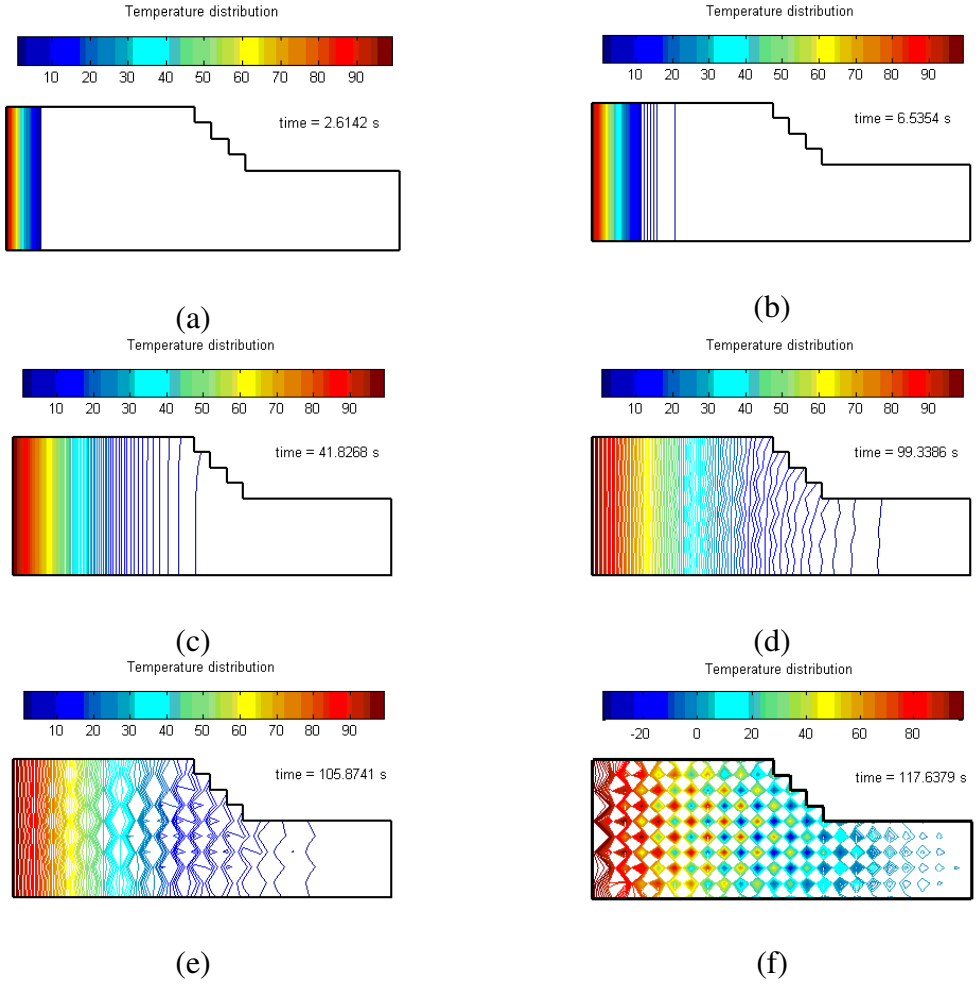

Figure 7.3. Unstable solution of transient 2D heat conduction problem for various instants in time is presented; at the very beginning everything looks fine, and temperature rises around the hot wall (a-c); after a certain number of time steps the solution starts to become disturbed (d); with more steps it becomes obvious that the solution has deviated very far from reality (f).

In the case of practical devices the computational domain is usually very complicated, containing small details. Therefore the spatial mesh has to be very fine (small steps Δx and

Δy). According to (7.25) this leads us to a very small value of time step $\Delta t_{\max}$ that ensures stability. With the small value of time step the method becomes very slow and dependent on the problem. Hence the stability condition can be considered the limiting factor for this method.
In 1974 [4] Crank and Nicholson proposed a solution to this problem in the form of an *implicit formula*. In the proposed solution the approximation of spatial partial derivatives (7.12) and (7.13) have been replaced by similar formulas containing the average value with respect to the time points *k* and *k+1* as follows:

$$\frac{\partial^2 T}{\partial x^2}(x,y,t) \overset{(5),(10)}{\approx} \frac{1}{2}\left[\frac{T(i+1,j,k)-2\cdot T(i,j,k)+T(i-1,j,k)}{(\Delta x)^2}+\frac{T(i+1,j,k+1)-2\cdot T(i,j,k+1)+T(i-1,j,k+1)}{(\Delta x)^2}\right] \tag{7.28}$$

$$\frac{\partial^2 T}{\partial y^2}(x,y,t) \overset{(5),(10)}{\approx} \frac{1}{2}\left[\frac{T(i,j+1,k)-2\cdot T(i,j,k)+T(i,j-1,k)}{(\Delta y)^2}+\frac{T(i,j+1,k+1)-2\cdot T(i,j,k+1)+T(i,j-1,k+1)}{(\Delta y)^2}\right] \tag{7.29}$$

Having approximations (7.28) and (7.29) at hand, equation (7.14) becomes:

$$\begin{aligned}&\lambda\frac{1}{2}\left[\frac{T(i+1,j,k)-2\cdot T(i,j,k)+T(i-1,j,k)}{(\Delta x)^2}+\frac{T(i+1,j,k+1)-2\cdot T(i,j,k+1)+T(i-1,j,k+1)}{(\Delta x)^2}\right]+\\&+\lambda\left[\frac{T(i,j+1,k)-2\cdot T(i,j,k)+T(i,j-1,k)}{(\Delta y)^2}+\frac{T(i,j+1,k+1)-2\cdot T(i,j,k+1)+T(i,j-1,k+1)}{(\Delta y)^2}\right]=\\&=\rho\cdot c_p\cdot\frac{T(i,j,k+1)-T(i,j,k)}{\Delta t}\end{aligned} \tag{7.30}$$

Using (7.15), equation (7.30) for an equidistant grid $\Delta x=\Delta y$ becomes:

$$\begin{aligned}&2(1+2r)\cdot T(i,j,k+1)-r\cdot\left[T(i+1,j,k+1)+T(i-1,j,k+1)+T(i,j+1,k+1)+T(i,j-1,k+1)\right]=\\&=2(1-2r)\cdot T(i,j,k)+r\cdot\left[T(i+1,j,k)+T(i-1,j,k)+T(i,j+1,k)+T(i,j-1,k)\right]\end{aligned} \tag{7.31}$$

Careful analysis of (7.31) shows that for *i=1,2,3,...,N* equation (7.31) defines a linear system of equations in which the unknowns are the values of temperature in the next step and the right hand side (RHS) is defined by known values of temperature from the previous step (in the first step the RHS is determined by the initial and boundary conditions). The basic advantage of this method is that an absolute stability is achieved [4]. A disadvantage is the fact that at each time step a large linear system has to be solved. Since the method's stability does not depend on the time step it can be larger than in the explicit formula. Hence the method is faster as well.
It is convenient to use such a time step that $r=1$ [4]:

$$\Delta t=\frac{\rho\cdot c_p\cdot\Delta x^2}{k} \tag{7.32}$$

In the case of our chosen material (7.24) the time step according to (7.32) is $\Delta t=4.35696s$ which is much larger than the maximum possible time step of the explicit algorithm (7.25). Consequently, the stationary solution of our problem depicted in Figure 7.1 can be reached with an acceptable accuracy within much less steps.

Taking into account formula (7.32), i.e. that $r=1$, the implicit formula (7.31) becomes far simpler:

$$\begin{aligned} &6\cdot T(i,j,k+1)-\left[T(i+1,j,k+1)+T(i-1,j,k+1)+T(i,j+1,k+1)+T(i,j-1,k+1)\right]= \\ &=-2\cdot T(i,j,k)+\left[T(i+1,j,k)+T(i-1,j,k)+T(i,j+1,k)+T(i,j-1,k)\right] \end{aligned} \tag{7.33}$$

The example from Figure 7.1 that was solved using the explicit formula (7.16) is used to check the efficiency of the implicit Crank-Nicholson formula (7.33). As one can see from (7.33) the matrix of the system of linear equations remains the same for all time steps and only the right-hand side is permanently changing. The matrix arising from (7.33) is a sparse matrix [6] and is depicted in Figure 7.4. If a direct matrix solver (for example Gaussian elimination [7] or LU factorization [7], etc.) is used, then the triangulated matrix or LU factors should be computed only once and used through all time steps. Sometimes the system of equations is so large that an iterative solver has to be used (for example GMRES or CG [6]) and linear system solution has to be performed at each time step.

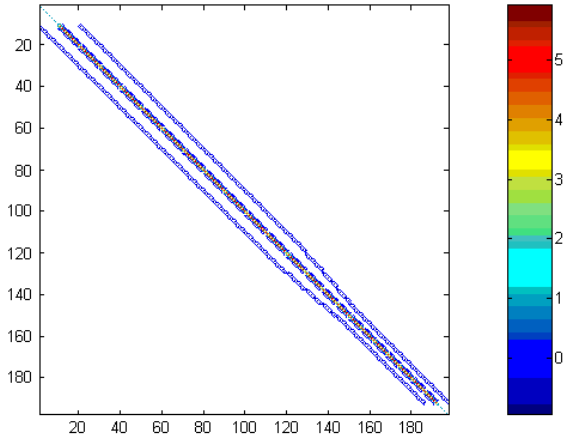

Figure 7.4. The structure of the matrix produced by (7.33) for the example shown in Figure 7.1; Coloured scale represents the scale of values of the matrix entries.

As one can see from Figure 7.4, many elements of the matrix are equal to zero (white area; blue zero value of the colorbar is replaced by white color for zero matrix entries) and only diagonal and some rare off-diagonal terms are non-zero. This structure is a consequence of equation (7.33). The non-zero terms describe the interactions between neighbors. Since the maximum number of neighbors for a regular grid is 4 and for boundary nodes can even be 2, it is clear why the matrix is sparse. The distribution of non-zero entities of the matrix depends directly on the node numbering scheme when the grid was generated.

In order to compare the efficiency of the implicit formula (7.33) against the explicit formula (7.16), two different cases, (d) and (f) from Figure 7.2, have been computed using implicit approach. These results are shown in Figure 7.5.

As one can see from Figure 7.5, solution (a) has been produced after only 16 iterations of the implicit formula. The corresponding solution of the explicit formula is shown in Figure 7.2 case (d) and took 79 iterations of the explicit formula. For solution (b), the situation is similar. The corresponding explicit solution in Figure 7.2f took 798 explicit iterations as opposed to only 160 iterations of the implicit formula. Obviously the stability condition for the explicit approach appears to be the significant drawback of the explicit method.

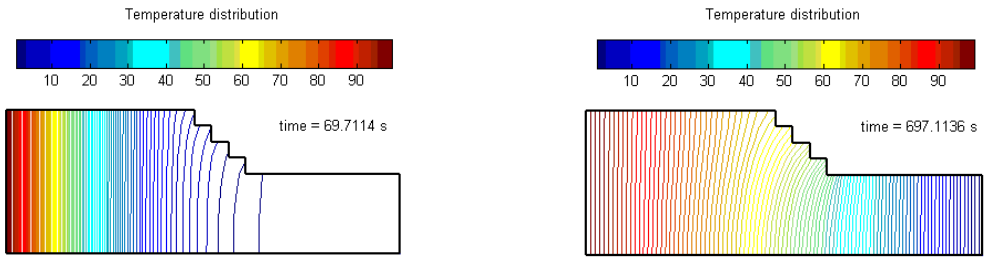

(7.a) (7.b)

Figure 7.5. The solutions obtained by using the implicit formula (7.33) are shown;
(a) Solution obtained after 16 steps of implicit formula;
(b) Solution obtained after 160 steps of implicit formula.

Using the suggested algorithms presented for 2D, in the case of parabolic PDEs the generalization to 3D should be fairly easy. The only difference is a slightly more complicated visualization of the results, as well as a larger number of neighbors for each single node in the grid.
There are many other approaches besides the two presented schemes (7.16) and (7.33) for parabolic PDEs. For further reading we recommend reference [4].

7.4. Hyperbolic PDEs and FDM (2D In-plane Wave Propagation)

The propagation of electromagnetic waves (EMWs) is described by a second order hyperbolic PDE. In order to present an application of FDM to this class of problems it is useful to start with a simple example. Therefore, a 2D problem of a parallel-plane waveguide defect and the propagation of the TM mode [8] will be analyzed. This is the so-called in-plane propagation (x-y plane is the propagation plane) where the z-component of the electric field is sufficient for the description of the electromagnetic wave propagation [9]:

$$\frac{\partial^2 E_z}{\partial x^2}+\frac{\partial^2 E_z}{\partial y^2}-\frac{1}{v^2}\frac{\partial^2 E_z}{\partial t^2}=0,\ v=\frac{1}{\sqrt{\mu\varepsilon}} \tag{7.34}$$

Wave equation (7.34) describes the field in a computational domain. Truncation of the structure is related, as we have already seen, to boundary conditions (BCs). In addition to the previously described BCs, here we have to introduce a new type of BC called the Absorbing Boundary Condition (ABC). In the case of electromagnetic waves the truncation of the structure (even at a large distance from the object of interest) produces a fictitious reflection of EMW that disturbs the accuracy of the computation. The role of an ABC is to truncate the structure in such a way that no fictitious reflection appears. Our analysis will start with a simple type of ABC, i.e. with the so-called first-order radiation boundary condition:

$$\frac{\partial E_z}{\partial n}+\frac{1}{v}\frac{\partial E_z}{\partial t}=0 \tag{7.35}$$

Our goal here is to approximate the differential operators in (7.34) and (7.35) and to derive the explicit formula for a 2D hyperbolic PDE.
Similar to (7.5) the second time derivative of E_z can be approximated as follows:

$$\frac{\partial^2 E_z}{\partial t^2}(x_i, y_j, t_k) \approx \frac{E_z(i,j,k+1) - 2 \cdot E_z(i,j,k) + E_z(i,j,k-1)}{(\Delta t)^2} \tag{7.36}$$

Using approximations (7.36), (7.12) and (7.13), equation (7.34) becomes:

$$\frac{E_z(i+1,j,k) - 2 \cdot E_z(i,j,k) + E_z(i-1,j,k)}{(\Delta x)^2} + \frac{E_z(i,j+1,k) - 2 \cdot E_z(i,j,k) + E_z(i,j-1,k)}{(\Delta y)^2} -$$
$$- \frac{1}{v^2} \frac{E_z(i,j,k+1) - 2 \cdot E_z(i,j,k) + E_z(i,j,k-1)}{(\Delta t)^2} = 0 \tag{7.37}$$

Similar to before, if the grid is equidistant in the x and y directions, i.e. if $\Delta x = \Delta y$, it is convenient and useful to introduce the following parameter:

$$r = \left(\frac{v \cdot \Delta t}{\Delta x} \right)^2 \tag{7.38}$$

Using (7.38) and some basic mathematical manipulations equation (7.37) can be written in the following explicit formula for 2D hyperbolic PDEs:

$$E_z(i,j,k+1) = r\left[E_z(i+1,j,k) + E_z(i-1,j,k) + E_z(i,j+1,k) + E_z(i,j-1,k) \right] +$$
$$+ 2\left(1 - 2 \cdot r\right) \cdot E_z(i,j,k) - E_z(i,j,k-1) \tag{7.39}$$

It is possible to show using the Fourier expansions technique that the stability condition of (7.39) is as follows [4]:

$$0 \le r \le \frac{1}{2} \Rightarrow \left(\frac{v \cdot \Delta t}{\Delta x} \right)^2 \le \frac{1}{2} \Rightarrow \boxed{\Delta t \le \frac{1}{\sqrt{2}} \frac{\Delta x}{v}} \tag{7.40}$$

ABC (7.35) has to be applied at the truncation boundary. The shape of this boundary is usually simple and we have freedom in its definition. Therefore it is very often a rectangular box around a scatterer[5] or a straight line representing the port of waveguide-like structures. In both cases the normal unit vector in (7.35) is either $\vec{e}_x$ or $\vec{e}_y$ and it is sufficient that we approximate equation (7.35) for the case when $\vec{n} = \vec{e}_x$, i.e. when (7.35) has the following form:

$$\frac{\partial E_z}{\partial x} \pm \frac{1}{v} \frac{\partial E_z}{\partial t} = 0 \tag{7.41}$$

The approximation of (7.41) depends on the situation, i.e. on the location of the boundary. Concerning this location there are two possible cases:

1. The computational domain is on the right-hand side of the absorbing boundary and the backward-difference formula (7.3) has to be applied:

[5] A scatterer is a body that scatters the incoming electromagnetic radiation

$$\frac{E_z(i,j,k)-E_z(i-1,j,k)}{\Delta x}-\frac{1}{v}\frac{E_z(i,j,k+1)-E_z(i,j,k)}{\Delta t}=0 \Rightarrow$$

$$\boxed{r\cdot E_z(i-1,j,k)=-\sqrt{r}\cdot E_z(i,j,k+1)+\sqrt{r}\cdot\left(1+\sqrt{r}\right)E_z(i,j,k)} \quad (7.42)$$

2. The computational domain is on the left-hand side of absorbing boundary and the forward-difference formula (7.2) has to be applied:

$$\frac{E_z(i+1,j,k)-E_z(i,j,k)}{\Delta x}+\frac{1}{v}\frac{E_z(i,j,k+1)-E_z(i,j,k)}{\Delta t}=0 \Rightarrow$$

$$\boxed{r\cdot E_z(i+1,j,k)=-\sqrt{r}\cdot E_z(i,j,k+1)+\sqrt{r}\cdot\left(1+\sqrt{r}\right)E_z(i,j,k)} \quad (7.43)$$

Having explicit formula (7.39) along with ABC (7.42, 7.43) one can solve 2D hyperbolic PDEs using FDM algorithm.
The parallel plane waveguide discontinuity presented in Figure 7.6 is used as a test example of the explicit approach (7.37).

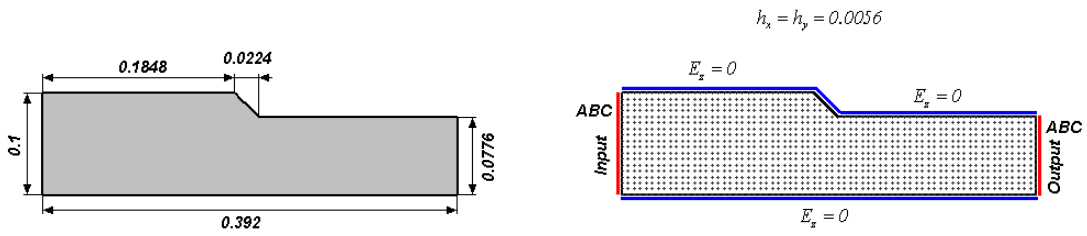

(a) (b)

Figure 7.7. 2D waveguide discontinuity problem: geometry, grid and BC definition;
(a) geometrical definition of the computational domain (all dimensions are given in meters)
(b) BC and FD grid definition (grid is equidistant in *x* and *y* direction, $h_x = h_y$)

Figure 7.6a shows the geometrical definition of the waveguide discontinuity problem and Figure 7.6b illustrates the grid definition and boundary conditions. The walls of the parallel plate waveguide structure are depicted in blue color and the corresponding boundary condition is of Dirichlet's type, i.e. the z-component of the electric field there is equal to zero. This comes from the fact that the walls of such a waveguide are considered to be perfect electric conductors (PECs) and the tangential electric field component is equal to zero over their surfaces [11]. The waveguide on the left-hand side of the structure as well as the waveguide on the right-hand side are considered to be infinitely long. Since our structure, i.e. the grid, must be of finite size, the computational domain has to be truncated at some distance from the discontinuity in both directions. These fictitious truncation boundaries are depicted in red color and along them the absorbing boundary conditions (7.42, 7.43) have to be applied. Having such boundary conditions our structure is now closed. The excitation of the structure, i.e. the source of electromagnetic field, can be defined and implemented using theoretical knowledge of a parallel-plane waveguide. Namely, if we choose to excite only the fundamental "even" TM mode, then the source field that represents the incoming wave at the input port has the following form:

$$E_z^{input}(0,y,t) = E_{z\,amp} \cdot \cos\left(\frac{\pi}{d_1} y\right) \cdot \sin\left(2\pi ft\right) \tag{7.44}$$

where the coordinate system is assumed to be in the middle of the input port, the *x*-axis is in the propagation direction, d_1 is the width of input waveguide and $E_{z\,amp}$ is the amplitude of the electric field for the incoming wave. The width of the waveguide will be reduced after the discontinuity from $d_1 = 0.1$ to $d_2 = 0.0776$. Consequently, the cut-off frequency of the fundamental even TM mode will be increased for the right-hand waveguide. Hence, if we want propagation in the right-hand side of the device the frequency of the input signal should be larger than the cut-off frequency of the right-hand side waveguide. From the basic theory of waveguides it is well known that the cut-off condition of the fundamental even TM mode for a parallel-plane waveguide is:

$$f \geq \frac{1}{2d\sqrt{\mu\varepsilon}} = \frac{v}{2d} \tag{7.45}$$

According to (7.45) the corresponding cut-off frequencies of our waveguides are $f_1 = 1.5 \cdot 10^9 Hz$ and $f_2 = 1.933 \cdot 10^9 Hz$. Hence we choose the operating frequency as $f = 2.7 \cdot 10^9 Hz$ in order to support guiding modes of both waveguides. It is possible to show that an acceptable accuracy in wave-propagation problems can be achieved only if the spatial grid has such resolution that a single field wavelength is covered by at least 10 points [4]. Consequently, we choose the grid to be equidistant in the x- and y-directions with the step $\Delta x = \Delta y = 0.0056m$. And finally the stability condition (7.40) will determine our time step:

$$\Delta t \leq \frac{1}{\sqrt{2}} \frac{\Delta x}{v} \;\Rightarrow\; \Delta t_{\max} = \frac{1}{\sqrt{2}} \frac{0.0056}{3 \cdot 10^8} = 1.3101 \cdot 10^{-11} s \tag{7.46}$$

We choose the time step by taking into account some “security” factor:

$$\Delta t = 0.8 \cdot \Delta t_{\max} = 1.0480 \cdot 10^{-11} s \tag{7.47}$$

Using previously mentioned parameters, explicit formula (7.39) has been used to solve the EMW propagation problem inside the waveguide structure shown in Figure 7.6a. The results are depicted in Figure 7.7. Obviously the solution is stable due to our “security” regarding conditions (7.46, 7.47). If we want to see what happens when stability condition (7.46) is not fulfilled it is enough to set the following time step:

$$\Delta t = 1.2 \cdot \Delta t_{\max} = 1.5721 \cdot 10^{-11} s \tag{7.48}$$

This unstable solution is shown in Figure 7.8. This effect was already explained when the parabolic PDE was analyzed. As opposed to the parabolic PDEs, the hyperbolic ones are rather different regarding the implicit schemes. Namely, according to the available literature, the implicit method for hyperbolic PDEs leads us to severe numerical difficulties that can be overcome using some simplifying assumptions [12]. Therefore for hyperbolic PDEs there is no elegant solution for the stability problem of the explicit approach as in the case of parabolic PDEs.

It is now worth mentioning that the truncation of the structure by using absorbing boundary conditions (ABCs) (7.42) and (7.43) works well only for certain modes and only when the incidence of waves is perpendicular to the boundary. Regarding the fact that we deal here with a regular grid the former condition usually can not be fulfilled. Therefore, extensive research within the FD scientific community has been performed in order to develop a more efficient ABC. Among very many suggested solutions Berenger's perfectly matched layers (PML) that work with a hypothetical absorbing material that does not exist in nature appears to be the most effective. For more information see textbooks on FD, for example [Taflove, 16], [Taflove, 17].

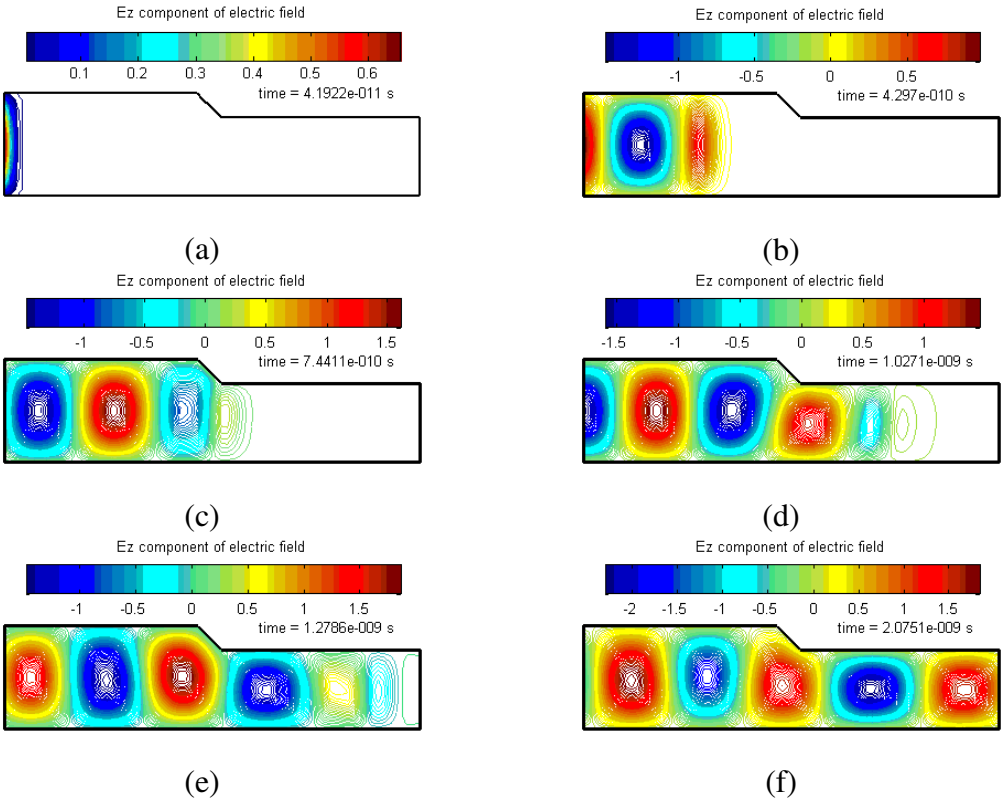

Figure 7.7. Solution of 2D electromagnetic propagation problem for various different instants of time is presented; At the very beginning only field at the input port exists (a); As time goes by, the electromagnetic wave penetrates into the waveguide, and the guiding mode appears (b); The wavefront reaches the waveguide defect (c); The guiding mode forms into the second waveguide (d); The wavefront reaches the output port (e); Stationary situation is established – EMW propagates through the structure (f).

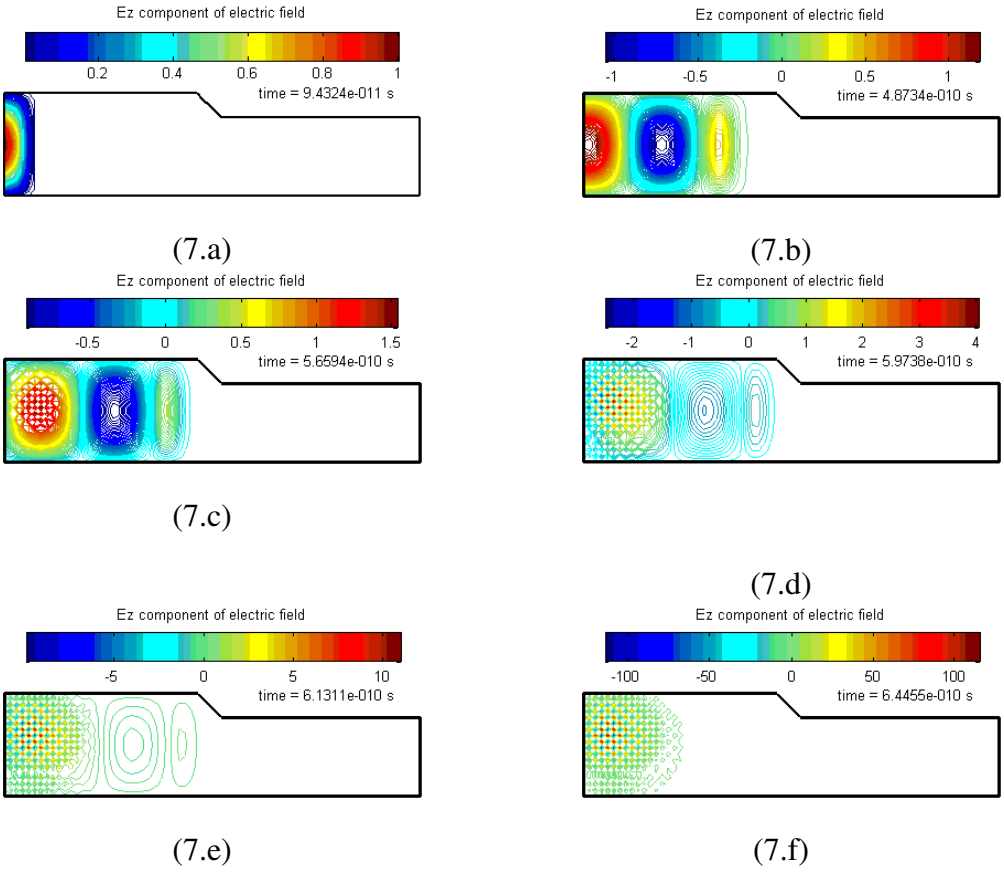

Figure 7.8. Unstable solution of 2D wave propagation problem for various different instants of time is presented; at the very beginning everything looks fine, and the EMW penetrates inside of waveguide structure (a-b); after a certain number of time steps the solution becomes disturbed (c-d); with more steps it is obvious that the solution deviates very far from reality (e-f).

7.5. Eliptic PDEs and FDM (2D Electrostatic Analysis)

Static fields such as electrostatic or magnetostatic fields are described by elliptic PDEs. In order to present the application of FDM to this type of PDE we will perform the electrostatic analysis of the shielded microstrip line depicted in Figure 7.9. This kind of analysis is very important for computation of a microstrip line's capacitance per unit length, which is then used for the computation of characteristic impedance and other transmission properties.

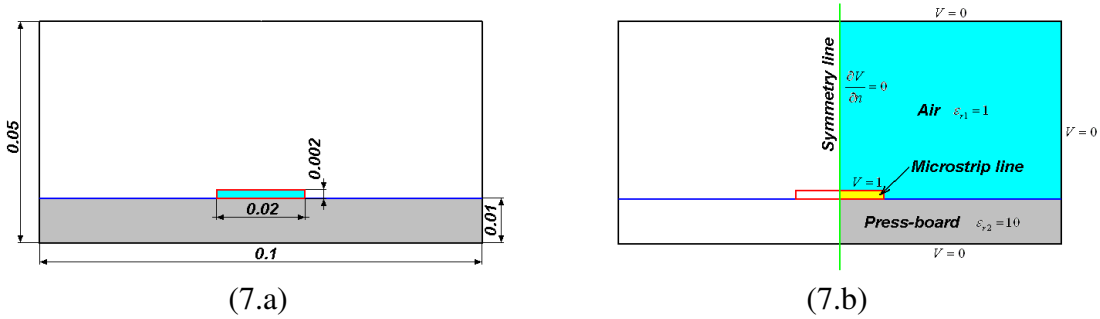

Figure 7.9. Example of 2D electrostatic analysis using FDM is shown; geometry and corresponding dimensions of the shielded microstrip line is depicted (a); due to the problem symmetry (green solid symmetry line) it is sufficient to analyze only half of the domain (b); electrical properties of materials along with the boundary conditions are given.

As one can see from Figure 7.9 the geometry is rather simple and appropriate for regular grid (rectangular shapes). At the top of the press-board (dielectric material of relative permittivity $\varepsilon_r = 10$) the thin strip consisting of conductive material (usually copper) is placed. Above the microstrip is air with relative permittivity of $\varepsilon_r = 1$. Everything is surrounded by a grounded metal shield (zero potential). The microstrip line is set to a potential of $V = 1V$ due to the fact that usually a voltage signal source is connected to the line at its very beginning. Figure 7.9b shows the symmetry line and consequently the problem size reduction to half of the original size. As we have already seen in electrostatics, for each homogenous and isotropic material one needs to solve the Laplace equation with corresponding boundary conditions:

$$\frac{\partial^2 V}{\partial x^2}(x,y) + \frac{\partial^2 V}{\partial y^2}(x,y) = 0\,,\ (x,y) \in \Omega \subseteq R^2 \tag{7.49}$$

$$V(x,y) = V_0(x,y)\,,\ (x,y) \in \partial_D \Omega \tag{7.50}$$

$$\frac{\partial V}{\partial n}(x,y) = q(x,y)\,,\ (x,y) \in \partial_N \Omega \tag{7.51}$$

where V is scalar electric potential, Ω represents the 2D computational domain, $\partial_D \Omega$ is the Dirichlet part of the domain boundary and $\partial_N \Omega$ represents the Neumann part of the boundary.
The first step of FDM application to this 2D electrostatic problem is a regular grid definition.

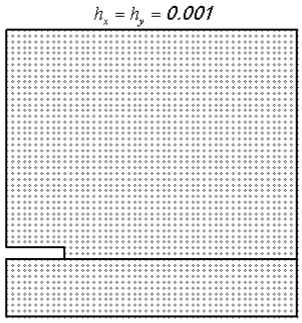

Figure 7.10. Regular grid generated over 2D computational domain is presented; grid is equidistant in x- and y-direction with step of 0.001m; number of nodes in the grid is 2601 (number of degrees of freedom (DOFs)); The region of the microstrip line is not covered by the grid because the field inside of the line (perfect conductor) is supposed to be zero (electrostatic analysis) and the outer boundary is at a known potential (Dirichlet's BC).

The next step of FDM application is to approximate equation (7.49) and boundary conditions (7.50-7.51) over the entire computational domain (Figure 7.9b). The second order partial derivatives in (7.49) can be approximated using equation (7.5) in the following way:

$$(49) \overset{(5,10)}{\Rightarrow} \quad V(i,j) = \frac{1}{4}\left[V(i-1,j) + V(i+1,j) + V(i,j-1) + V(i,j+1)\right] \tag{7.52}$$

Equation (7.52) can only be used for internal points in the domain of air or in the domain of the press-board. At the interface between the two dielectric materials (blue line in Figure 7.9a) the situation is a bit more complicated because of different permittivities from both sides of

the interface. In order to derive the equation valid over the interface we will use an integral form of Gauss's law:

$$\oint_{(L)} \varepsilon \frac{\partial V}{\partial n} dl = 0 \tag{7.53}$$

Since the problem is 2D, the surface integral of Gauss's law in 3D is here replaced by line integral in (7.53). This is illustrated in Figure 7.11.

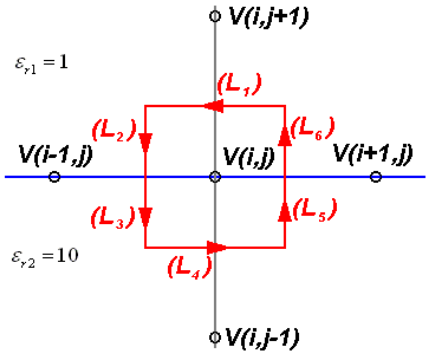

Figure 7.11. The node is at the interface between two dielectric materials; the integration over the red line has to be performed over parts belonging to one single material.

By following the integration path presented in Figure 7.11, equation (7.53) can be written as follows:

$$\oint_{(L)} \varepsilon \frac{\partial V}{\partial n} dl = \varepsilon_1 \int_{(L_1)} \frac{\partial V}{\partial n} dl + \varepsilon_1 \int_{(L_2)} \frac{\partial V}{\partial n} dl + \varepsilon_2 \int_{(L_3)} \frac{\partial V}{\partial n} dl + \varepsilon_2 \int_{(L_4)} \frac{\partial V}{\partial n} dl + \varepsilon_2 \int_{(L_5)} \frac{\partial V}{\partial n} dl + \varepsilon_1 \int_{(L_6)} \frac{\partial V}{\partial n} dl = 0 \tag{7.54}$$

The partial derivatives inside integrals in (7.54) can easily be approximated by finite differences as follows:

$$\begin{aligned} &\varepsilon_1 \frac{V(i,j+1)-V(i,j)}{h} \cdot h + \varepsilon_1 \frac{V(i-1,j)-V(i,j)}{h} \cdot \frac{h}{2} + \\ &+\varepsilon_2 \frac{V(i-1,j)-V(i,j)}{h} \cdot \frac{h}{2} + \varepsilon_2 \frac{V(i,j-1)-V(i,j)}{h} \cdot h + \varepsilon_2 \frac{V(i+1,j)-V(i,j)}{h} \cdot \frac{h}{2} + \\ &+\varepsilon_1 \frac{V(i+1,j)-V(i,j)}{h} \cdot \frac{h}{2} = 0 \end{aligned} \tag{7.55}$$

After some basic mathematical manipulations equation (7.55) can be written as follows:

$$V(i,j) = \frac{1}{4} V(i-1,j) + \frac{1}{4} V(i+1,j) + \frac{\varepsilon_1}{2(\varepsilon_1+\varepsilon_2)} V(i,j+1) + \frac{\varepsilon_2}{2(\varepsilon_1+\varepsilon_2)} V(i,j-1) \tag{7.56}$$

For all points over the interface between the two dielectrics equation (7.56) is used. Using a similar procedure one can derive the interface condition for any other geometric interface configuration.

If the grid's node is located on the symmetry line, Neumann boundary condition (7.51) has to be used. In terms of finite differences it reduces (7.51) to the following form:

$$\frac{\partial V}{\partial n}=\frac{\partial V}{\partial x}=\frac{V(i+1,j)-V(i-1,j)}{2h}=0 \;\Rightarrow\; V(i-1,j)=V(i+1,j) \tag{7.57}$$

Using equation (7.57) it is possible to transform (7.52) into the form appropriate for the points over the interface:

$$(52)\overset{(57)}{\Rightarrow}\; V(i,j)=\frac{1}{4}\left[2\cdot V(i+1,j)+V(i,j-1)+V(i,j+1)\right] \tag{7.58}$$

So for each point of the grid one can either write (7.52), (7.56) or (7.58) depending on whether the point is inside the domain, at the interface or on the symmetry line respectively. We have practically obtained a large system of equations with the potential values in nodes as unknowns. The nodes over the Dirichlet boundaries have known potential and consequently those equations can be replaced with a simple identity (the corresponding potential equals the corresponding value). The described procedure has been performed for the electrostatic example from Figure 7.9 using the grid from Figure 7.10. The obtained matrix is depicted in Figure 7.12.

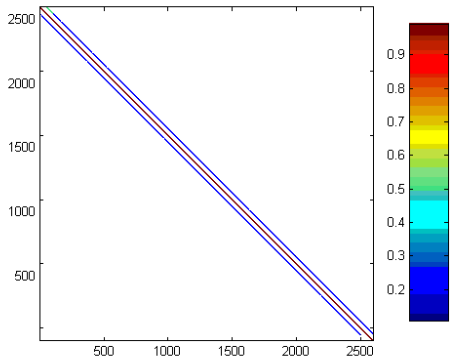

Figure 7.12. The matrix of the linear system described by equations (7.52), (7.56) and (7.58) is depicted; absolute values of matrix entries are presented; size of matrix is 2601x2601.

The matrix is obviously sparse (with very many zero entries) and can be solved by either using direct (Gaussian elimination) or iterative (GMRES or BiCG) method. Since the matrix here is not very large we have used the direct solver. The obtained solution is shown in Figure 7.13.

After the solution in terms of static electric potential is computed one can easily compute the capacitance per unit length by calculating the electrostatic energy.

The presented method is relatively simple, easy to use, and can be generalized to 3D without additional difficulties.

7. 7. FDTD algorithm (2D In-plane Wave Propagation)

The FDM application to hyperbolic PDEs has already been presented in Section 4, i.e. the wave propagation problems were under consideration. The wave equation in the case of in-plane propagation has been treated and the approximation of second order partial derivatives was required. An attempt to generalize this approach to 3D will lead us to a fairly complicated structure of 3 hyperbolic PDEs for each vector component. In order to deal with a simpler structure and in order to directly approximate Maxwell's equations (first order partial derivatives) instead of wave equations (second order partial derivatives) the finite difference time domain (FDTD) algorithm was proposed by Yee in 1966 [13]. The basic idea and advantage of this algorithm is a usage of central-difference scheme (7.4) for all derivatives in space and time. At the very beginning it was shown that the central-difference scheme has better accuracy than the forward- and backward-difference schemes. As will be seen later, Yee introduced an artifice – called leap frog scheme - that allows him to use the central-difference scheme for the time derivatives in Maxwell's differential equations directly. In order to have a simple picture, it is useful to start with a 2D example of TM mode propagation in a parallel plate waveguide.

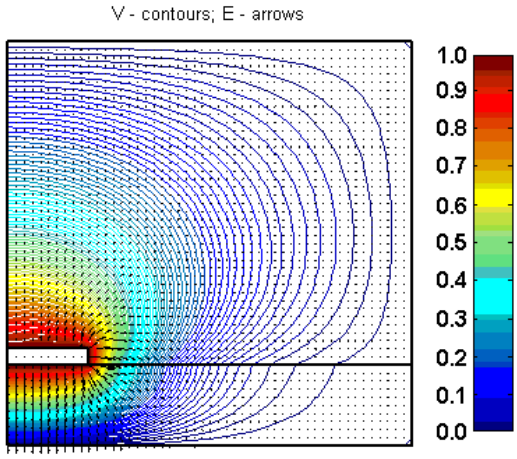

Figure 7.13. Obtained solution is shown; contour lines represent the scalar electric potential; arrows represent the vectors of electric field (arrow size is related to the field intensity).

.

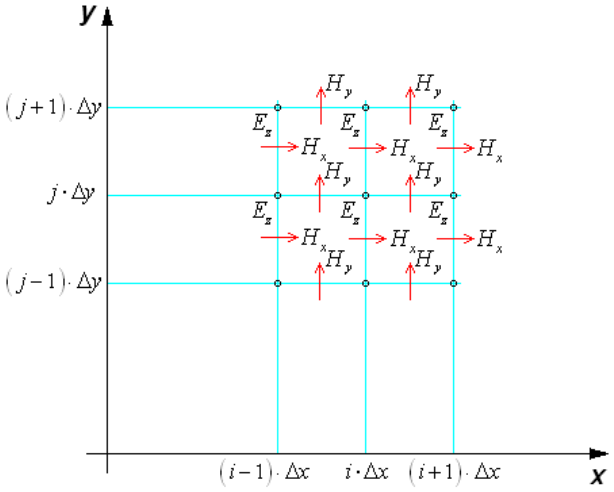

Figure 7.14. 2D FDTD algorithm for TM mode propagation; E_z is related to the nodes of the grid and H_x, H_y components of the magnetic field are related to the mid points between the nodes.

In the case of in-plane propagation of the TM mode the Maxwell curl equations can be reduced to the following form:

$$\frac{\partial E_z}{\partial y} = -\mu \frac{\partial H_x}{\partial t} \tag{7.59}$$

$$\frac{\partial E_z}{\partial x} = \mu \frac{\partial H_y}{\partial t} \tag{7.60}$$

$$\varepsilon \frac{\partial E_z}{\partial t} = \frac{\partial H_y}{\partial x} - \frac{\partial H_x}{\partial y} \tag{7.61}$$

The first order partial derivatives in (7.59-61) can be easily approximated in the following way:

$$\frac{E_z(i,j+1,k) - E_z(i,j,k)}{\Delta y} = -\mu \frac{H_x\left(i,j+\frac{1}{2},k+\frac{1}{2}\right) - H_x\left(i,j+\frac{1}{2},k-\frac{1}{2}\right)}{\Delta t} \tag{7.62}$$

$$\frac{E_z(i+1,j,k) - E_z(i,j,k)}{\Delta x} = \mu \frac{H_y\left(i+\frac{1}{2},j,k+\frac{1}{2}\right) - H_y\left(i+\frac{1}{2},j,k-\frac{1}{2}\right)}{\Delta t} \tag{7.63}$$

$$\varepsilon \frac{E_z(i,j,k+1) - E_z(i,j,k)}{\Delta t} = \\ = \frac{H_y\left(i+\frac{1}{2},j,k+\frac{1}{2}\right) - H_y\left(i-\frac{1}{2},j,k+\frac{1}{2}\right)}{\Delta x} - \frac{H_x\left(i,j+\frac{1}{2},k+\frac{1}{2}\right) - H_x\left(i,j-\frac{1}{2},k+\frac{1}{2}\right)}{\Delta y} \tag{7.64}$$

or in a more appropriate way:

$$H_x\left(i, j+\frac{1}{2}, k+\frac{1}{2}\right) = H_x\left(i, j+\frac{1}{2}, k-\frac{1}{2}\right) + \frac{\Delta t}{\mu \cdot \Delta y}\left[E_z\left(i, j, k\right) - E_z\left(i, j+1, k\right)\right] \tag{7.65}$$

$$H_y\left(i+\frac{1}{2}, j, k+\frac{1}{2}\right) = H_y\left(i+\frac{1}{2}, j, k-\frac{1}{2}\right) + \frac{\Delta t}{\mu \cdot \Delta x}\left[E_z\left(i+1, j, k\right) - E_z\left(i, j, k\right)\right] \tag{7.66}$$

$$\begin{aligned} E_z\left(i, j, k+1\right) = E_z\left(i, j, k\right) + \frac{\Delta t}{\varepsilon \cdot \Delta x}\left[H_y\left(i+\frac{1}{2}, j, k+\frac{1}{2}\right) - H_y\left(i-\frac{1}{2}, j, k+\frac{1}{2}\right)\right] - \\ - \frac{\Delta t}{\varepsilon \cdot \Delta y}\left[H_x\left(i, j+\frac{1}{2}, k+\frac{1}{2}\right) - H_x\left(i, j-\frac{1}{2}, k+\frac{1}{2}\right)\right] \end{aligned} \tag{7.67}$$

Note that these finite differences look like forward differences but they are in fact central differences because the different field components are evaluated at different nodes of the grid! For example, in (7.62) The E_z components are evaluated on the nodes, whereas the H_x components are evaluated half way in between. Similarly, the $\vec{E}$ field components are evaluated at time steps, k, k+1, etc. and the $\vec{H}$ field components half way in between. Also note that half time steps are used to ensure central differences for the time derivatives. The update procedure is the following: when the field is known for time step k (and before, namely k-1/2), one applies (7.65) and (7.66) to update the H field for time step k+1/2. After this, one updates the E field using (7.67) and obtains the field at time step k+1. This alternating H and E field update procedure is called the leap frog scheme. It has the following stability condition [4]:

$$v_{\max} \cdot \Delta t \le \left[\frac{1}{\Delta x^2} + \frac{1}{\Delta y^2}\right]^{-\frac{1}{2}} \tag{7.68}$$

which for an equidistant mesh in the x- and y- directions can be written in a simpler way:

$$\frac{v_{\max} \cdot \Delta t}{\Delta x} \le \frac{1}{\sqrt{2}} \tag{7.69}$$

where $v_{\max}$ is the maximum phase velocity of waves appearing in the structure.

The leap frog scheme can easily be extended to 3D problems. One then has 6 field components and 6 update equations that are derived from the Maxwell curl equations. Note that the remaining Maxwell divergence equations are implicitly satisfied. The leap frog scheme becomes more complicated when 1) lossy, 2) dispersive (frequency dependent), and 3) anisotropic materials are present. One then needs to introduce additional field components and obtains additional or more complicated update equations. When doing this, one must be careful to always ensure second order accuracy by only using central differences. For more information, see [16, 17].

A simple class of absorbing boundary conditions (7.52) and (7.53) can be applied here as well, although a special class of highly effective absorbing boundary conditions – the so-called Perfectly Matched Layers (PMLs) , see [16, 17] – are used in all modern FDTD codes.

The example presented in Figure 7.6 may be used here as well to illustrate FDTD. Using stability condition (7.51) the time step has been selected in the following way:

$$\Delta t = 0.8 \cdot \Delta t_{\max}\ ,\ \Delta t_{\max} = \frac{1}{\sqrt{2}} \frac{\Delta x}{v_{\max}} \tag{7.70}$$

An additional advantage here is that besides the z-component of the electric field, the magnetic field components are also known, as shown in Figure 7.15.

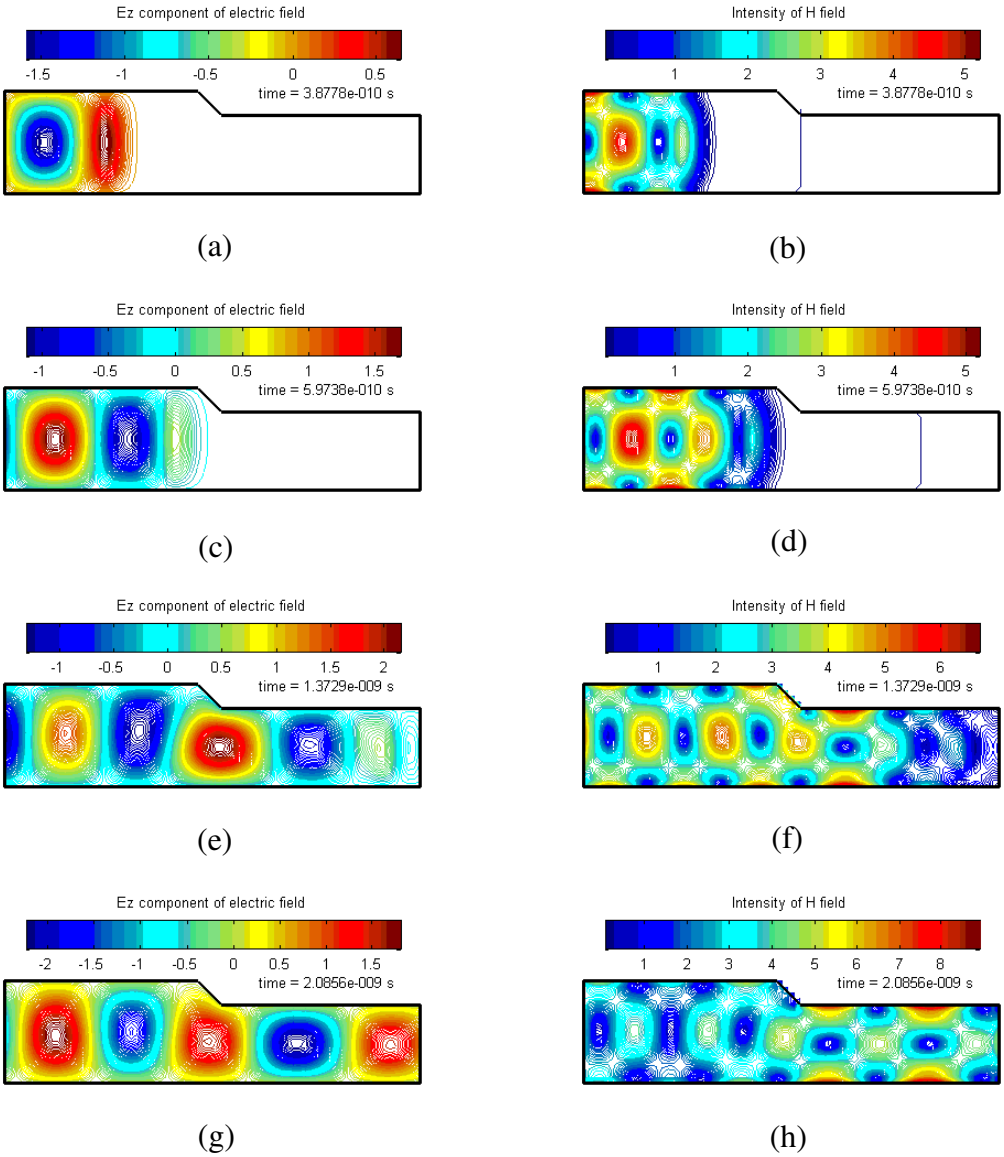

Figure 7.15. Stable solution of a 2D wave propagation problem using the FDTD algorithm for various different instants of time is presented; z-component of electric field (a, c, e, g) and intensity of magnetic field (b, d, f, h) is presented.

7.7. Finite Integral (FI) Technique

After the theory presented in the previous sections it is obvious that deriving FD and FDTD schemes is most simple when regular grids that coincide with Cartesian coordinates are used. The main drawback of such grids is that they do not nicely follow curved boundaries and

therefore may cause the so-called staircasing effect. The main problems related with FD and FDTD schemes for irregular grids are [11]:

1. Much additional information on the location of the grid points must be stored, whereas the location of the grid points can be easily evaluated for regular or slightly irregular grids.
2. The development of appropriate FD operators is difficult.
3. The numerical evaluation of the resulting schemes requires considerably more computation time than the evaluation of the simple schemes on regular grids,
4. Because of the central differences formulation, even simple FD schemes on regular grids may be of second order, whereas the simplest FD schemes on irregular grids are only first order and therefore have a reduced accuracy.

In order to overcome the second problem mentioned above, the Finite Integral (FI) technique was proposed [14]. Its idea is simple. Instead of using the Maxwell equations in differential form one uses their integral form for the derivation of the upgrade schemes. The grid lines can then be used as a path for those integrals and therefore no regular grid is required. In order to illustrate this, we will derive equation (7.64) starting from the corresponding Maxwell equation in integral form:

$$\oint_{(C)} \vec{H}\left(\vec{r},t\right)\cdot d\vec{l} = \iint_{(S)} \frac{\partial}{\partial t}\left[\varepsilon\vec{E}(\vec{r},t)\right]\cdot d\vec{S} \tag{7.71}$$

With Figure 7.14 one easily finds:

$$\begin{aligned} &H_y(i+\frac{1}{2},j,k+\frac{1}{2})\cdot\Delta y - H_x(i,j+\frac{1}{2},k+\frac{1}{2})\cdot\Delta x - H_y(i-\frac{1}{2},j,k+\frac{1}{2})\cdot\Delta y + \\ &+H_x(i,j-\frac{1}{2},k+\frac{1}{2})\cdot\Delta x = \varepsilon\frac{E_z\left(i,j,k+1\right)-E_z\left(i,j,k\right)}{\Delta t}\Delta x\cdot\Delta y \end{aligned} \tag{7.72}$$

For this derivation it was assumed that the magnetic field along the sides of the integration rectangle is constant as well as the electric field over the rectangular surface. The FI technique is implemented in the Microwave Studio code from CST [15].

Note that there is no essential difference between the FI equation (7.72) and the corresponding FD equation (7.64). This is no surprise because the physical content of the Maxwell equation in integral form is exactly the same as the content of the Maxwell equation in differential form. What differs is the way the update scheme is derived. Yee himself pointed out that he also was inspired by pictures of the integral formulations when he invented the leap frog scheme. For this reason, most researchers currently use the terms FD and FDTD, no matter whether they work with the differential or integral formulations of Maxwell's equations.

7.8. Concluding Remarks

Different 2D FD algorithms were outlined. Deriving similar 3D algorithms is straightforward and poses no essential problems. In addition to the FD scheme itself, powerful FD codes need many additional features that are difficult to implement and finally result in very large source codes. We have already mentioned the problems of lossy, dispersive, and anisotropic media as well as the problem of ABCs such as PMLs. Additionally, time-domain codes usually need

Fourier transforms and similar techniques (for example, harmonic inversion) because many properties of practical interest are defined in the frequency domain. Although the Fourier transform is well known, its implementation in FDTD codes is not trivial, especially when accurate results should be obtained without large computer resources (memory and computation time).

7.9 References

[1] A. Thom, C. J. Apelt, "Field Computations in Engineering and Physics", D. Van Nostrand, London, 1961.

[2] E. W. Weisstein, "Finite Difference." From MathWorld--A Wolfram Web Resource. http://mathworld.wolfram.com/FiniteDifference.html

[3] R. W. Lewis, P. Nithiarasu, K. N. Seetharamu, "Fundamentals of the Finite Element Method for Heat and Fluid Flow", John Wiley & Sons Ltd, San Francisco, 2004.

[4] M. N. O. Sadiku, "Numerical Techniques in Electromagnetics", CRC Press, Boca Raton, 2001.

[5] D. R. Lide, "CRC Handbook of Chemistry and Physics", 86th Edition, CRC Press, Boca Raton, 2005-2007.

[6] Y. Saad, "Iterative Methods for Sparse Linear Systems", 2nd Edition, SIAM (Society for Industrial and Applied Mathematics) and University of Chicago, Chicago, 2003.

[7] G. H. Golub, Ch. F. Van Loan, "Matrix Computations", 3rd Edition, The Johns Hopkins University Press, Baltimore, 1997.

[8] J. D. Jackson, "Classical Electrodynamics", Third Edition, John Wiley & Sons, Chichester, 1999.

[9] D. M. Sullivan, "Electromagnetic Simulation Using the FDTD Method", IEEE Press, New York, 2000.

[10] D. D. Davidson, "Computational Electromagnetics for RF and Microwave Engineering", Cambridge University Press, Cambridge, 2005.

[11] Ch. Hafner, Post-modern Electromagnetics, Wiley & Sons, New York, 1999.

[12] G. D. Smith, "Numerical Solution of Partial Differential Equations: Finite Difference Methods", 3rd edition, Oxford University Press, New York, 1985.

[13] K. S. Yee, "Numerical Solution of Initial Boundary-Value Problems Involving Maxwell's Equations in Isotropic Media", IEEE Trans. Ant. Prop., vol. AP-14, pp. 302-307, 1967.

[14] T. Weiland, "A discretization method for the solution of Maxwell's equations for six-component Field," Electronics and Communications AEUE, vol. 31, no. 3, pp. 116-120, 1977.

[15] Microwave Studio, the code based on Finite Integral (FI) technique, http://www.cst.de.

[16] A. Taflove: Computational Electrodynamics: The Finite-Difference Time-Domain Method, Artech House, Norwood, MA, 1995.

[17] A. Taflove: Advances in Computational Electrodynamics: The Finite-Difference Time-Domain Method, Artech House, Norwood, MA, 1998.